Phase Behavior in Self-Assembly of Inorganic/ Poly(4-vinylpyridine)-*b*-poly(ε-caprolactone) Hybrid

Tao Lin,[†] Rong-Ming Ho,*[,†,‡] and Jia-Chong Ho[§]

Institute of Nanoengineering and Microsystems and Department of Chemical Engineering, National Tsing-Hua University, Hsinchu 30013, Taiwan and Electronics Research & Service Organization, Industrial Technology Research Institute, Hsinchu 30013, Taiwan

Received July 11, 2008; Revised Manuscript Received November 17, 2008

ABSTRACT: A series of poly(4-vinylpyridine)-*b*-poly(ε-caprolactone) (P4VP-PCL) diblock copolymers of different composition (namely, various nanostructured phases) were synthesized for hybridization with gold precursors. Interesting phase behavior of gold precursors/P4VP-PCL hybrids was found as evidenced by transmission electron microscopy and small-angle X-ray scattering (SAXS). Consistent with theoretical prediction, phase transformation in the hybrids with PCL-rich P4VP-PCL can be induced by the introduction of the gold precursors. In particular, the phase transformation can be achieved by introducing a very small amount of the gold precursors because of the significant increase in the effective excluded volume of hybridized P4VP microdomain as identified by SAXS experiments through the analysis of the 1D correlation function. This morphological evolution is referred to as the bridging mechanism, suggesting that the PCL block of the P4VP-PCL in the hybrids might play an important role in blocking the interconnection between hybridized P4VP microdomains. In contrast, disordered morphology was observed in the hybrids with P4VP-rich P4VP-PCL because of the strong association between the gold precursors and the P4VP block that might disrupt the ordered phase from microphase separation.

Introduction

Hybridization of inorganic and organic materials is a promising approach to increase the great diversity of applied materials[1−13] such as metal−organic frameworks[12] and ionic liquid-block copolymer composites.[13] Because of the stability and excellent physical properties possessed by the inorganic materials, especially the high electrical conductivity and catalytic capability, inorganic species (regardless of ionic precursors or elemental nanoparticles) are designed to disperse uniformly within the organic matrix to render the composites with potential applications such as organic thin-film transistor[14] and gas sorption.[15] For hybridization, the self-assembly of block copolymers (BCPs) has become an attractive candidate as an organic template to attract, separate, and arrange the inorganic materials because of the functional constituent groups and rich geometric nanostructures.

Recently, a systematic theoretical study in the self-assembly of inorganic/BCP hybrids has been carried out by Ginzburg, Balazs, Matsen, and coworkers. They predicted that the affinity, size, and amount of inorganic nanoparticles can be exploited to control the phase behavior of inorganic/BCP hybrids under strong segregation limit. Moreover, a simulated phase diagram of inorganic/BCP hybrids revealed that phase transformation can be induced by the introduction of nanoparticles.[16−18] Also, the strength of affinity governed by prewetting block−nanoparticle interaction may lead to the disruption of microphase separation. Interestingly, the simulated phase diagram of inorganic/BCP hybrids qualitatively agreed with theoretical calculations for the phase behavior of homopolymer/BCP blends[19] and selective solvent/BCP mixtures[20] at which the low-molecular-weight homopolymers and selective solvent in the blends presumably act much like small particles in the hybrids.

Over the years, many experimental designs focused on tuning the location of functional nanoparticles so as to improve the physical properties of polymeric materials as nanocomposites via BCP templation.[10,21−24] A convenient method is to modify the surface properties of insoluble metallic nanoparticles by ex situ presynthesis and surface modification for hybridization. Such an approach makes it easy to control the size of metallic nanoparticles so as to define the dispersion of nanoparticles. Thomas and coworkers demonstrated the formation of hierarchical hybrid patterns using poly((styrene)-*block*-ethylene propylene) (PS-PEP) diblock copolymers and binary inorganic mixtures (AuR_1 and SiO_2R_2) with hydrophobic nanoparticles of different size.[21] Wei and coworkers examined the morphological transformation from cylinder phase to lamellar phase in poly((styrene)-*block*-4-vinylpyridine) (PS-P4VP) diblock copolymers through the hybridization with modified CdS quantum dots.[10] Kramer and coworkers examined the phase transformation by hybridizing the presynthesized gold nanoparticles and poly((styrene)-*block*-2-vinylpyridine) (PS-P2VP) diblock copolymers.[22] This approach took advantage of the chemically attractive interaction between the BCP and the functionalized nanoparticle surface so as to allocate the nanoparticle in the hybrids precisely.

In contrast, in situ hybridization by directly hybridizing inorganic precursors and BCPs can also be used to examine the effective interaction through the time-resolved reduction of the formation of inorganic nanoparticles templated by BCP self-assembly.[25−30] Also, in situ hybridization involves synthesizing nanoparticles in situ within preformed BCP microdomains from microphase separation. Preformed micelles of the BCPs containing metal precursors can be used as nanoreactors for selectively synthesizing nanoparticles in the BCPs. Hashimoto and coworkers traced the Pd dispersion formed within the P2VP microdomains in the self-assembly of poly((2-vinylpyridine)-*block*-isoprene) (P2VP-PI) by in situ hybridization.[25] Moreover, Cohen and coworkers produced regular silver nanoarrays via the templation of poly((styrene)-*block*-acrylic acid) (PS-PAA). Recently, Lodge and coworkers combined the ionic liquid and poly((butadiene-*block*-ethylene oxide) (PB-PEO) to form ion

* To whom correspondence should be addressed. Tel: 886-3-5738349. Fax: 886-3-5715408. E-mail: rmho@mx.nthu.edu.tw.
[†] Institute of Nanoengineering and Microsystems, National Tsing-Hua University.
[‡] Department of Chemical Engineering, National Tsing-Hua University.
[§] Industrial Technology Research Institute.

10.1021/ma8015618 CCC: $40.75
Published on Web 01/16/2009

Table 1. Characterization of P4VP-PCL Diblock Copolymers

sample	M_n^{P4VP} (g/mol)[a]	M_n^{PCL} (g/mol)[a]	M_n^{total} (g/mol)	f_{P4VP}	PDI[b]	morphology
V2C7	2000	7000	9000	0.24	1.25	cylinder
V3C7	2800	7000	9800	0.30	1.27	cylinder
V3C5	2900	5400	8300	0.37	1.25	cylinder
V4C7	4000	7000	11 000	0.38	1.24	cylinder
V5C5	5000	5400	10 400	0.50	1.27	lamellae
V15C5	15 000	5400	20 400	0.75	1.28	cylinder
V22C5	21 600	5400	27 000	0.81	1.29	cylinder

[a] M_n^{P4VP} and M_n^{PCL} were characterized by proton nuclear magnetic resonance (^{1}H NMR). [b] The polydispersity index (PDI) in the diblock copolymers was determined by GPC using standard calibration.

gels with practical applications[28,29] in which the phase behavior of ion gels has been studied through cryo-transmission electron microscopy (cryo-TEM) and small-angle X-ray scattering (SAXS) experiments.[28,29] Through the identification of the disorder-to-order transition (DOT) in lithium salt/poly((styrene)-*block*-methylmethacrylate) (PS-PMMA) hybrids, Russell and coworkers suggested that the overall segmental interaction, especially for the entropic part, is significantly increased as a result of ionic complex formation.[31,32]

In our previous work, similar to the phase transformation observed in the ex situ hybridization, interesting morphological evolution can be observed by the introduction of various amounts of gold precursors to poly(4-vinylpyridine)-*block*-ε-caprolactone) (P4VP-PCL) diblock copolymers.[26] As observed, phase transformation from the cylinder phase to the lamellar phase can be clearly identified in gold precursors/P4VP-PCL hybrids, as evidenced by TEM and SAXS experiments. Obviously, systematic experimental examination in the phase diagram of inorganic/BCP hybrids is necessary for practical applications. In this study, we aim to investigate the phase behavior of inorganic/BCP hybrids by examining a series of P4VP-PCL BCPs of different compositions (namely, various nanostructured phases). In contrast to the theoretical prediction, interesting phase behavior was found; phase transformation in the hybrids with PCL-rich P4VP-PCL can be induced by the introduction of the gold precursors whereas disordered morphology was observed in the hybrids with P4VP-rich P4VP-PCL. Also, it is noted that the phase transformation can be achieved by the introduction of a very small amount of the gold precursors. It leads to the question of how significant the effective excluded volume of the gold precursors will be to cause the phase transformation. Quantitative analysis on the effective excluded volume was carried out by SAXS experiments through the analysis of the 1D correlation function. Consequently, the mechanism for the phase transformation behavior was examined, suggesting that the PCL block of the P4VP-PCL in the hybrids may play an important role in blocking the strong association of gold precursors and P4VP chains through microphase separation.

Experimental Section

Materials. A series of BCPs, P4VP-PCL, was synthesized via living ring-opening and atom transfer radical polymerization in sequence.[33,34] The molecular characteristics and the sample codes of the P4VP-PCL BCPs are listed in Table 1.

Nanostructures of P4VP-PCL. Bulk samples of pristine BCPs were prepared by solution-casting method using dichloromethane (CH_2Cl_2) solution (10 wt % of P4VP-PCL) at room temperature. To eliminate possible effects of PCL crystallization and residual solvent on the microphase-separated morphology during solvent evaporation, we annealed all bulk samples at 140 °C, which is above the glass-transition temperature of the P4VP block ($T_{g,P4VP} \approx 100$ °C) and well above the equilibrium melting point ($T_{m^\circ,PCL} = 69$ °C) of PCL block but below the estimated order−disorder-transition temperature ($T_{ODT} \approx 230$ °C)[35] for 12 h under a nitrogen atmosphere. After thermal treatment, the samples were rapidly cooled at a rate of 150 °C/min to room temperature. Subsequently, the samples were examined by both TEM and SAXS experiments (Figures S1 and S2 in the Supporting Information). In Figure S1a−c in the Supporting Information, a well-ordered hexagonally packed cylinder phase can be observed in the V2C7, V3C5, and V4C7 with $f_{P4VP}{}^{v} = 0.24$, 37, and 0.38, respectively, at which the P4VP microdomains appear to be dark and the PCL microdomains appear to be bright. Corresponding SAXS patterns further confirm the observed phases according to the scattering peaks that occurred at characteristic q^* ratios of $1{:}\sqrt{3}{:}\sqrt{4}$ (Figure S2a,c in the Supporting Information). With the increase in the P4VP volume fraction to symmetric composition (V5C5 ($f_{P4VP}{}^{v} = 0.5$)), the lamellar phase can be found (Figure S1d in the Supporting Information). The typical lamellar phase exhibits the q^* ratio of 1:2:3 (Figure S2d in the Supporting Information) in the SAXS profile. Further increasing the volume fraction of the P4VP, the inverse cylinder phase can be identified by the TEM images at which dark P4VP microdomains are dispersed in the bright matrix PCL (Figure S1e,f in the Supporting Information for V15C5 ($f_{P4VP}{}^{v} = 0.75$) and V22C5 ($f_{P4VP}{}^{v} = 0.81$), respectively). The corresponding SAXS profiles with the q^* ratios of $1{:}\sqrt{3}{:}\sqrt{4}$ are in line with the TEM observation (Figure S2e,f in the Supporting Information). In contrast to the results examined under ambient condition, it is noted that the intensity of the primary peak significantly increases and the breadth of the peaks becomes narrow at temperatures above the melting point of the PCL block, as illustrated by the dashed line in Figure S2a,c in the Supporting Information, for which the SAXS profiles were recorded at 70 °C to eliminate the PCL crystallites. The variation of the scattering peaks in the SAXS results is referred to as the effect of PCL crystallization at which the electron density within the PCL domains is less uniform than that in the melt after the crystallization of PCL block.[33] As a result, the P4VP-PCL samples of different composition (namely, various nanostructured phases) were synthesized and characterized.

Inorganic/P4VP-PCL Hybridization. A common gold precursor, hydrogen tetrachloroaurate trihydrate ($HAuCl_4$), was used as an inorganic species to incorporate with the P4VP-PCL for the formation of hybridized materials. Taking advantage of the association between the nitrogen lone-pair electrons and the gold precursors, the hybridization of the gold precursors and the P4VP-PCL can be simply achieved by solution mixing using dichloromethane (CH_2Cl_2) solution (1 wt % gold/P4VP-PCL) with a specific ratio of nitrogen on the P4VP block to gold precursors (Au/N). The solution was stirred for 1 day to allow for the complete solubilization of the gold precursors. The bulk samples of gold precursors/P4VP-PCL hybrids were prepared by casting from the prepared solutions. The cast samples were then thermally treated by following a procedure similar to that for neat BCP samples that was previously described.

The added amount of the gold precursors was defined by the stoichiometry of the Au/N ratio to determine the degree of association. For the hybridization of the gold precursors and the P4VP-PCL, the experimental observation indicated that the gold precursors were indissoluble in the CH_2Cl_2 solution. In contrast, the polymer solution can lead the gold precursors to be dissolved in the CH_2Cl_2 solution. This result suggests that the P4VP-PCL acts as a surfactant so as to improve the solubility of gold precursors in the CH_2Cl_2 solution significantly. As a result, the harmony of hybridization can be achieved by the incorporation of the gold precursors and the P4VP block. To trace the reliability of hybridization further, infrared (IR) spectra analysis was used. The appearance of extra bands such as 1637 and 1506 cm^{-1} in the Fourier transform infrared (FTIR) spectra of the hybrids (results not shown) compared with those of neat P4VP-PCL is attributed to the association of the pyridine units at which unsaturated gold precursors can be coordinated to the nitrogen lone-pair electrons of P4VP.[26] As a result, we suggest that the association of the gold precursors with the pyridine units in the P4VP block can be achieved.

Instrumental Details. *Differential Scanning Calorimetry.* Differential Scanning Calorimetry (DSC) experiments were carried out on a Perkin-Elmer DSC 7 equipped with an intracooler and

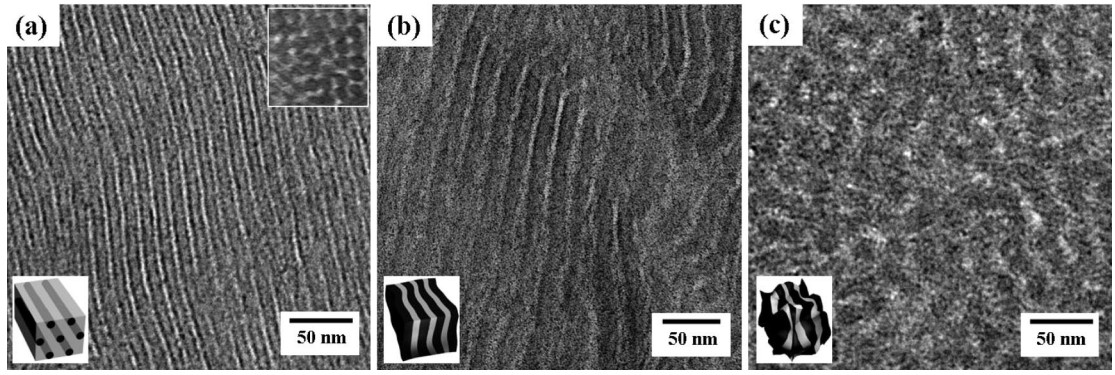

Figure 1. TEM micrographs of (a) V4C7 ($f_{P4VP}^{\nu} = 0.38$), (b) gold precursors/V4C7 (Au/N 1/7), and (c) gold precursors/V4C7 (Au/N 1/3). All samples were stained by RuO_4 at which the dark region represents the P4VP microdomain and the bright region represents the PCL microdomain. The micrograph in the inset of Figure 1a shows the TEM projection along the cylinders.

calibrated with cyclohexane and indium for the measurements of thermal behavior of P4VP-PCL.

Transmission Electron Microscopy. Bright field TEM images were obtained using the mass−thickness contrast with a JEOL TEM-1200x (at an accelerating voltage of 120 kV). Ultrathin sectioning (50−60 nm) was performed by ultramicrotomy (Leica Ultracut R) with a cooling system (Leica EMFCS) at −100 °C. Staining was accomplished by exposing the samples to the vapor of a 4% aqueous RuO4 solution for 30 min.

Small-Angle X-ray Scattering. SAXS profiles (log (q) versus q ($= 4\pi \sin(\theta/2)/\lambda$), here q is the scattering vector and θ is the scattering angle) were conducted at the beamline BL17B3 of the National Synchrotron Radiation Research Center (NSRRC). The incident X-ray beam was focused vertically by a mirror and monochromated to the energy of 10 keV by a Germanium (111) double-crystal monochromator. The wavelength of the X-ray beam was 1.24 Å. The beam stop was a round tantalum disk that was 4 mm in diameter. A MAR CCD X-ray detector (MAR) was used to collect the 2D SAXS patterns. The scattering angle of the SAXS pattern was calibrated using silver behenate. A 1D linear profile was obtained by azumuthally integrating the reflections on the 2D pattern. The normalized 1D correlation function used in this study is given by

$$\gamma(z) = \frac{1}{Q}\int_0^\infty q^2 I(q)\cos(qz)\,\mathrm{d}q$$

where z is the coordinate along which the electron density distribution is measured, q is the scattering vector, $I(q)$ is the 1D intensity, and Q is the integrated scattering intensity defined by

$$Q = \int_0^\infty q^2 I(q)\,\mathrm{d}q$$

To fit the 1D correlation function, the scattering intensity was first corrected for background scattering. The scattering intensity by thermal fluctuations was subtracted from the SAXS profile $I(q)$ by evaluating the slope of $I(q)q4$ versus $q4$ plots at wide scattering vectors q. Then, the plots of the correlation function ($\gamma(z)$) versus real space coordinate (z) data were calculated using the normalized 1D correlation function. To identify the characteristic spacing for the thinner layer, the intercept (for the real space coordinate axis) was calculated by the tangent line near the position at $z = 0$. We note that the crystallinity of the PCL might cause the variation of the results of the 1D correlation function. To eliminate the disturbance of crystallization, all samples were heated to >70 °C (the melting point of PCL segment is ~55 °C). FTIR experiments were collected on a Perkin-Elmer system-2000 spectrometer at a resolution of 1 cm^{-1}. The films for FTIR measurements were prepared by casting solution on KBr salt and were dried to prevent the disturbance of water. The experiments were carried out at room temperature (25 °C).

Results and Discussion

Phase Behavior of Gold Precursors/P4VP-PCL Hybrids. Our previous results for the hybrids of V3C5 ($f_{P4VP}^{\nu} = 0.37$) indicated that interesting morphological evolution can be observed, at which the introduction of gold precursors was preferentially associated with the P4VP microdomains and thus induced the transformation of the cylinder phase to the lamellar phase.[26] To generalize the phase transformation behavior, we prepared various P4VP-PCL samples so as to examine the effects of polymer properties such as molecular weight and constituent composition on the phase behavior of inorganic/P4VP-PCL hybrids. To examine the molecular weight effect on the phase transformation, we synthesized V4C7 (f_{P4VP}^{ν} =0.38) with similar constituent composition to V3C5 (f_{P4VP}^{ν} =0.37) but higher molecular weight for hybridization through a similar procedure for sample preparation. As shown in Figure 1, the intrinsic cylinder phase of the V4C7 ($f_{P4VP}^{\nu} = 0.38$) (Figure 1a) can be modified by the addition of the gold precursors, and it finally transforms to the lamellar phase (Figure 1b) once the added amount of the gold precursors reaches the critical value of Au/N 1/7. When the concentration of the gold precursors is further increased, the lamellar morphology gradually becomes a lamellae-like morphology with distorted texture (Figure 1c). Also, it was noted that the occurrence of the phase transformation usually corresponds to the occurrence of diffused boundaries at the microphase-separated interface. We speculate that the corresponding changes in the morphologies of hybrids are attributed to the strong association between gold precursors and P4VP chains. (See below for reasons.) A comparison of the results of the morphological evolution in the V4C7 (f_{P4VP}^{ν} = 0.38) hybrids to a previous study of the V3C5 ($f_{P4VP}^{\nu} = 0.37$) hybrids shows that the ordered microphase-separated phase could remain by the introduction of a larger amount of the gold precursors in the V4C7 ($f_{P4VP}^{\nu} = 0.38$) hybrids. This result indicates that the BCP system with higher segregation strength, namely, higher molecular weight, possesses higher stability for the formation of ordered hybridized phase. To examine the phase behavior of the hybrids, in particular, the composition effect, further, P4VP-PCL with large asymmetric constituent composition (that is, V2C7 ($f_{P4VP}^{\nu} = 0.24$)) was used for hybridization. Consistently, a significant phase transformation from the cylinder phase to the lamellar phase and finally diffused lamellae can be observed in the gold precursor/V2C7 hybrids (Figure 2a−c).

Moreover, the evolution of the phase transformation for the gold precursor/P4VP-PCL hybrids was examined by SAXS experiments (Figure 3). Consistent with the TEM results, as shown in Figure 3a for the gold precursors/V4C7 hybrids, the reflections of the original cylinder phase dramatically change with the introduction of the gold precursors; eventually, the

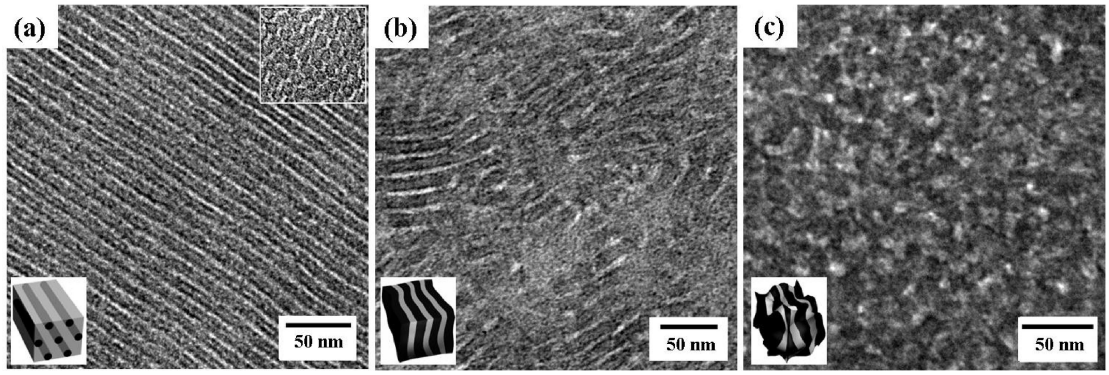

Figure 2. TEM micrographs of (a) V2C7 ($f_{P4VP}{}^{\nu} = 0.24$), (b) gold precursors/V2C7 (Au/N 1/7), and (c) gold precursors/V2C7 (Au/N 1/3). All samples were stained by RuO_4 at which the dark region represents the P4VP microdomain and the bright region is the PCL microdomain. The micrograph in the inset of Figure 2a shows the TEM projection along the cylinders.

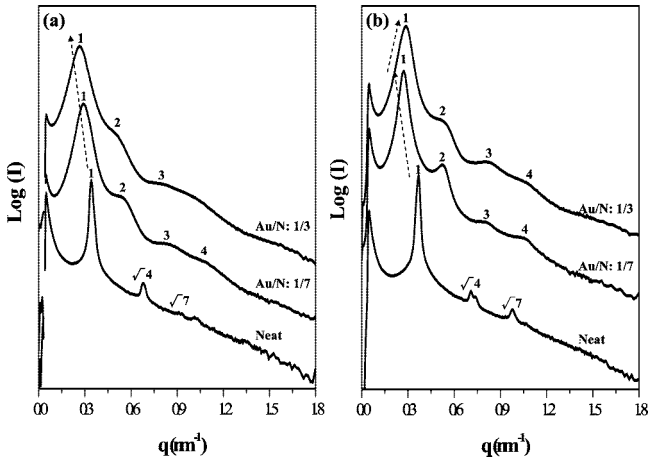

Figure 3. One-dimensional SAXS profiles of (a) V4C7 ($f_{P4VP}{}^{\nu} = 0.38$) and its hybrids and (b) V2C7 ($f_{P4VP}{}^{\nu} = 0.24$) and its hybrids.

cylindrical characteristic peak ratio transfers to the lamellar peak ratio at the concentration of the gold precursors with Au/N 1/7. Similarly, in the gold precursors/V2C7 hybrids, the suggested phase transformation from TEM observations can be evidenced by SAXS (Figure 3b). Furthermore, the scattering intensity of the SAXS profiles dramatically decreases by further increasing the concentration of the gold precursors; we speculate that the decrease is attributed to the occurrence of large-degree distortion on microphase-separated texture caused by the formation of diffused boundaries, as observed by TEM. Consequently, on the basis of the TEM and SAXS results, the phase transformation from the cylinder phase to the lamellar phase is a characteristic behavior for the gold precursors/P4VP-PCL hybrids.

Nevertheless, it is remarkable that the primary reflection in the V4C7 ($f_{P4VP}{}^{\nu} = 0.38$) gradually shifts to lower q (namely, larger long-period spacing) with the increase in the concentration of the gold precursors, whereas the change in the primary reflection of the V2C7 ($f_{P4VP}{}^{\nu} = 0.24$) hybrids appears to be an unusual variation (Figure 3b). In general, the increase in the long-period spacing is referred to as the swelling effect attributed to the introduction of the gold precursors because the gold precursors are preferentially associated with the P4VP microdomains. In contrast with the increase in the long-period spacing in the V4C7 ($f_{P4VP}{}^{\nu} = 0.38$) hybrids with the introduction of the gold precursors, the V2C7 ($f_{P4VP}{}^{\nu} = 0.24$) hybrids with high loading of gold precursors (for instance Au/N 1/3) revealed a decrease in the long-period spacing. Further increasing the gold precursors concentration in the V2C7 ($f_{P4VP}{}^{\nu} = 0.24$) would lead to the segregation of the gold precursors, as observed by TEM (results no shown), whereas no significant segregation for the gold precursors could be found in the V4C7 ($f_{P4VP}{}^{\nu} = 0.38$) hybrids with the same level of gold precursors concentration. It is intuitive to suggest that the P4VP-PCL with a longer P4VP block such as V4C7 ($f_{P4VP}{}^{\nu} = 0.38$) may play a role in stabilizing the hybridized morphology so that there is a higher solubility limit for the introduced gold precursors in the V4C7 ($f_{P4VP}{}^{\nu} = 0.38$). Note that how to increase the concentration for hybridization is always a critical issue for the consideration of practical applications. It raises the question of whether it is possible to increase the hybridized concentration by using P4VP-rich P4VP-PCL because of the matter of the longer P4VP block. To scrutinize the suggested phase behavior further, the P4VP-PCL hybrids with P4VP-rich fractions (V22C5 ($f_{P4VP}{}^{\nu} = 0.81$) and V15C5 ($f_{P4VP}{}^{\nu} = 0.75$)) were synthesized for hybridization. In contrast, instead of phase transformation, disordered morphology occurred even when a small amount of the gold precursors was introduced, for instance, the V15C5 ($f_{P4VP}{}^{\nu} = 0.75$) hybrids with Au/N 1/14. As shown in Figure 4, original PCL cylinders in the P4VP matrix (Figure 4a) are directly transferred to the disordered morphology with irregular texture (Figure 4b). When the concentration of the gold precursors was further increased, both cases encountered significant segregation of gold precursors, suggesting that the solubility limit can be easily reached by the introduction of relatively small amounts of the gold precursors. For instance, the segregation of gold precursors/P4VP-PCL hybrids can be observed in the V15C5 ($f_{P4VP}{}^{\nu} = 0.75$) and V22C5 ($f_{P4VP}{}^{\nu} = 0.81$) with Au/N 1/7, indicating that BCPs with minor PCL composition are difficult for maintaining the solubility of the gold precursors in hybrids.

For the formation of the disordered morphology, we speculate that this is attributed to the strong association of the gold precursors and the P4VP block. This strong association can be explicitly evidenced by the precipitation experiments. The gold precursors and P4VP homopolymer were dissolved in methanol (which is a good solvent for both P4VP homopolymers and gold precursors). In contrast with the clear solution of the P4VP homopolymer and the gold precursors, the solution mixing of the hybrids might lead to significant precipitation attributed to the formation of P4VP colloidal gel upon mixing with the gold precursors (Figure 4) because of the strong aggregation of P4VP chains with high-density gold precursors (3.9 g/cm^3). Similar phase behavior has been observed by Ruehrwein and Ward, and they suggested that the significant precipitation as polymeric flocculants is referred to as the bridging mechanism attributed to the strong association of solutes such as polymer chains and ions.[36] In the polymer/ion mixing solution, the contact of polymer chains and free ions can be easily achieved by many kinds of driving force such as Lewis acid−base interaction. Through the contacts among polymeric attached sites (several attached sites on each polymer chain) and free ions, well-defined

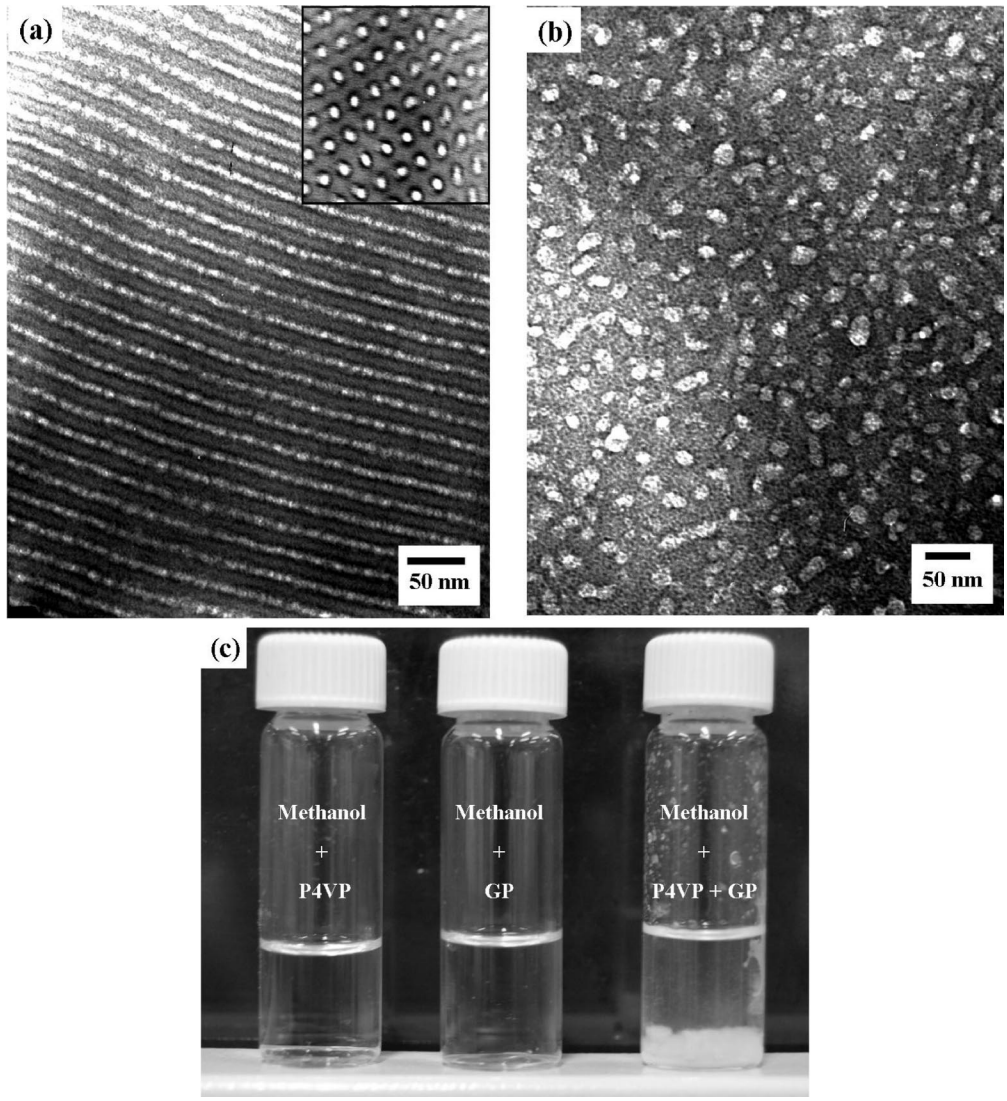

Figure 4. TEM micrographs of (a) V15C5 ($f_{P4VP}{}^{\nu} = 0.75$) and (b) gold precursors/V15C5 (Au/N 1/14) with RuO_4 staining. (c) Solutions of methanol and P4VP homopolymer (left), methanol and gold precursors (center), and methanol, P4VP homopolymer and gold precursors (right). The micrograph in the inset of Figure 4a shows the TEM projection along the cylinders.

polymer/ion mixtures can be obtained in which the long polymer chains play the role of the bridge to interconnect with neighboring ions; it is referred to as the bridging mechanism. Similar to the described behavior, we speculate that the significant precipitation in the solution of gold precursor/P4VP-PCL hybrids is attributed to the strong association between the gold precursors and the P4VP block at which each P4VP block might associate with many ions (i.e., the gold precursors).

Effective Excluded Volume. According to the theoretical prediction, there is similarity in the phase transformation behaviors of the inorganic nanoparticle/BCP hybrids, the homopolymer/BCP blends, and selective solvent/BCP mixtures. Nevertheless, the swelling behavior in the hybrid system studied here exhibits quite different results from those of the above cases in which the phase transformation can be achieved by the introduction of a very small amount of the gold precursors. For instance, it is a ca. 0.022 to 0.042 fraction of the gold precursors in volume, as calculated from the added amount and the density of the gold precursors, to lead a significant phase transformation. In the case of the hybrids of V2C7 ($f_{P4VP}{}^{\nu} = 0.24$) with Au/N 1/7, the volume fraction of the gold precursors introduced is only ca. 0.022. Nevertheless, according to the phase transformation from the cylinder phase to the lamellar phase, the apparent change in the volume fraction of P4VP microdomains should be significant. Obviously, the gold precursors strongly affect the surrounding pyridine chains and lead to the significant increase in excluded volume. The apparent excluded volume is thus defined as effective excluded volume for hybridization. Instead of simple swelling by the intrinsic volume of the gold precursors, the association of the gold precursors and the lone pair of nitrogen in the P4VP profoundly creates extra volume in the P4VP microdomains so as to cause the phase transformation.

To resolve the effective excluded volume of the gold precursors in the hybrids, the volume fraction of the hybridized P4VP microdomains was calculated by the 1D correlation function from the SAXS results. On the basis of the assumption, the dispersion of the gold precursors within the P4VP microdomains is uniformly distributed to form the ideal binary system. By tracing the profile of the 1D correlation function, it is convenient to calculate the thicknesses for both hybridized P4VP and PCL microdomains. As shown in Figure 5, the plots of the correlation function ($\gamma(z)$) versus real space coordinate (z) data are calculated using the normalized 1D correlation function. In the case of the V4C7 ($f_{P4VP}{}^{\nu} = 0.38$) hybrids (Figure 5a), the correlation function reveals that the profile of the hybrids is modified to a symmetric composition. Thus, the thickness of the thinner layer and the long period are determined to be 7.9

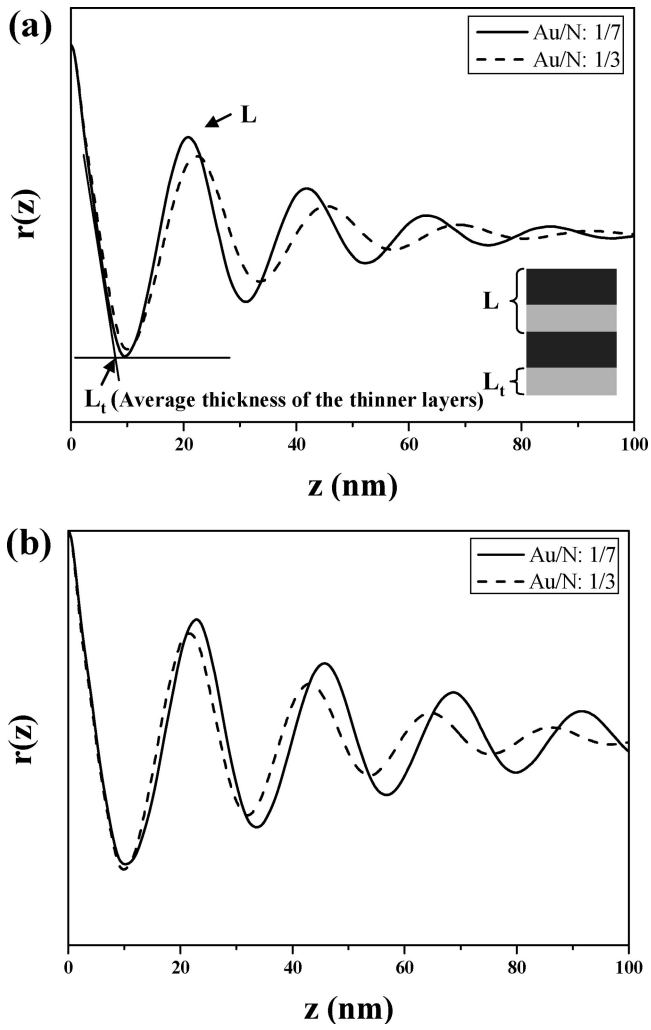

Figure 5. One-dimensional correlation function of (a) gold precursors/V4C7 hybrids and (b) gold precursors/V2C7 hybrids. The thickness of lamellar long period was calculated by the position of first peak and the average thickness of the thinner layers was determined by the connection between tangent and baseline of the first wave trough.

and 20.8 nm for the hybrids with Au/N 1/7 and 8.2 and 22.4 nm for the hybrid with Au/N 1/3, respectively. As a result, we suggest that the thinner layer should be referred to as the thickness of the PCL microdomain according to the changes in the long periods for hybrids with Au/N 1/7 and Au/N 1/3 and also the approximate invariant value of 8.0 nm thickness for the PCL microdomains with different amounts of the gold precursors. Obviously, the calculated results show that the interaction between the gold precursors and the P4VP block significantly enhances the excluded volume. For instance, in the hybrids of V2C7 ($f_{P4VP}{}^{\nu} = 0.24$) with Au/N 1/7, the effective excluded volume fraction (volume fraction of hybridized P4VP microdomain – volume fraction of neat P4VP microdomain) could reach ca. 0.39 by only the introduction of 0.022 gold precursors in volume. Also, the swelling of V2C7 ($f_{P4VP}{}^{\nu} = 0.24$) hybrids reveals a different profile from that of the V4C7 ($f_{P4VP}{}^{\nu} = 0.38$) hybrids (Figure 5b). In contrast with the simple swelling in the V4C7 ($f_{P4VP}{}^{\nu} = 0.38$) hybrids, the long period of V2L7 ($f_{P4VP}{}^{\nu} = 0.24$) hybrids decreases from 22.9 to 21.6 nm for the hybrids with Au/N 1/7 and Au/N 1/3. To unravel the changes in lone periods in the V4C7 and V2C7 hybrids with the gold precursors introduced further, it is important to trace the mechanism of the phase transformation induced by hybridization. Also, the formation of significant aggregation in the P4VP-rich P4VP-PCL hybrids (V15C5 and V22C5) drew our attention to examine the transformed mechanism of the hybrids.

Mechanism of Phase Transformation. Considering the significant changes in the phase morphologies caused by the introduction of the gold precursors, a very small amount of gold precursors (for instance, Au/N 1/30) was introduced to the V2C7 hybrids to realize the mechanism for the corresponding phase transformation. The TEM image indicates that the original hexagonally packed cylinders (Figure 6a) are transferred to the intermediate stage (Figure 6b), and then the morphology with significant coalescence by interconnection can be clearly identified (Figure 6c). Such interconnection among neighboring cylinders is achieved by decreasing the mean curvatures of the interface and hence leading to the lower Gibbs free-energy state. On the basis of the TEM observations, this phase transformation from the cylinder phase to the lamellar phase suggests that the hybrids reach the lamellar phase though the interconnection of neighboring cylinders instead of the rearrangement of microphase separation from the disorder state.

A similar transforming mechanism (interconnection of neighboring cylinders) from the cylinder phase to the lamellar phase has been proposed by Sakurai and coworkers according to the systematic observations in thermally induced phase transition in poly((styrene)-*block*-butadiene-*block*-styrene) (SBS) copolymers.[37] Figure 6d schematically illustrates the change in the free energy involved in the morphological transformation. Along with the transitional path via the disordered state, the free-energy barrier is considerably large because of the complete mixing of strongly repulsive PCL and hybridized P4VP chains (dotted curve). In contrast, the energy barrier for the intermediate state by interconnection is expected to be relatively small because of smaller interfacial contact between PCL and hybridized P4VP microdomains (solid curve). In contrast with the phase transformation of the SBS triblock copolymers, we speculate that the driving force results from the multiattached sites for the association of the gold precursors and the P4VP block (i.e., each P4VP block might associate with many gold precursors and vice versa). Consequently, the multiattached sites for the association of the gold precursors and the P4VP block might lead to the significant increase in the effective excluded volume so as to cause the phase transformation through the interconnection of neighboring hybridized P4VP chains, namely, the bridging mechanism.

PCL Blocking versus Bridging. According to the results of 1D correlation function analyses, as shown in Figure 7a, a significant increase in the effective excluded volume of the hybridized P4VP microdomain can be obtained by the introduction of gold precursors to the V2C7 ($f_{P4VP}{}^{\nu} = 0.24$) hybrids. In contrast, in the V4C7 ($f_{P4VP}{}^{\nu} = 0.38$) hybrids, the change in the effective excluded volume is not dramatic. We hypothesize that the intrinsic interdistance of neighboring cylinders in the P4VP-PCL may govern the energy barrier for the phase transformation from the cylinder phase to the lamellar phase. Namely, the bridging mechanism through the association of the gold precursors and the P4VP block is justified by the PCL chain length. The restraint for the interconnection of hybridized P4VP microdomains attributed to the PCL microdomain is referred to as the PCL blocking effect for the bridging of hybridized P4VP chains, and the interdistance of neighboring cylinders is the effective distance of PCL blocking. As a result, because of a larger intercylinder distance (~9.4 vs ~7.4 nm) (Figure 7b), it is much more difficult for the interconnection of neighboring hybridized P4VP microdomains in the V2C7 ($f_{P4VP}{}^{\nu} = 0.24$) hybrids than for that in the V4C7 ($f_{P4VP}{}^{\nu} = 0.38$) hybrids. Subsequently, a large increase in the effective excluded volume can be found in the V2C7 ($f_{P4VP}{}^{\nu} = 0.24$) because of the larger energy barrier for the interconnection. Eventually, the P4VP

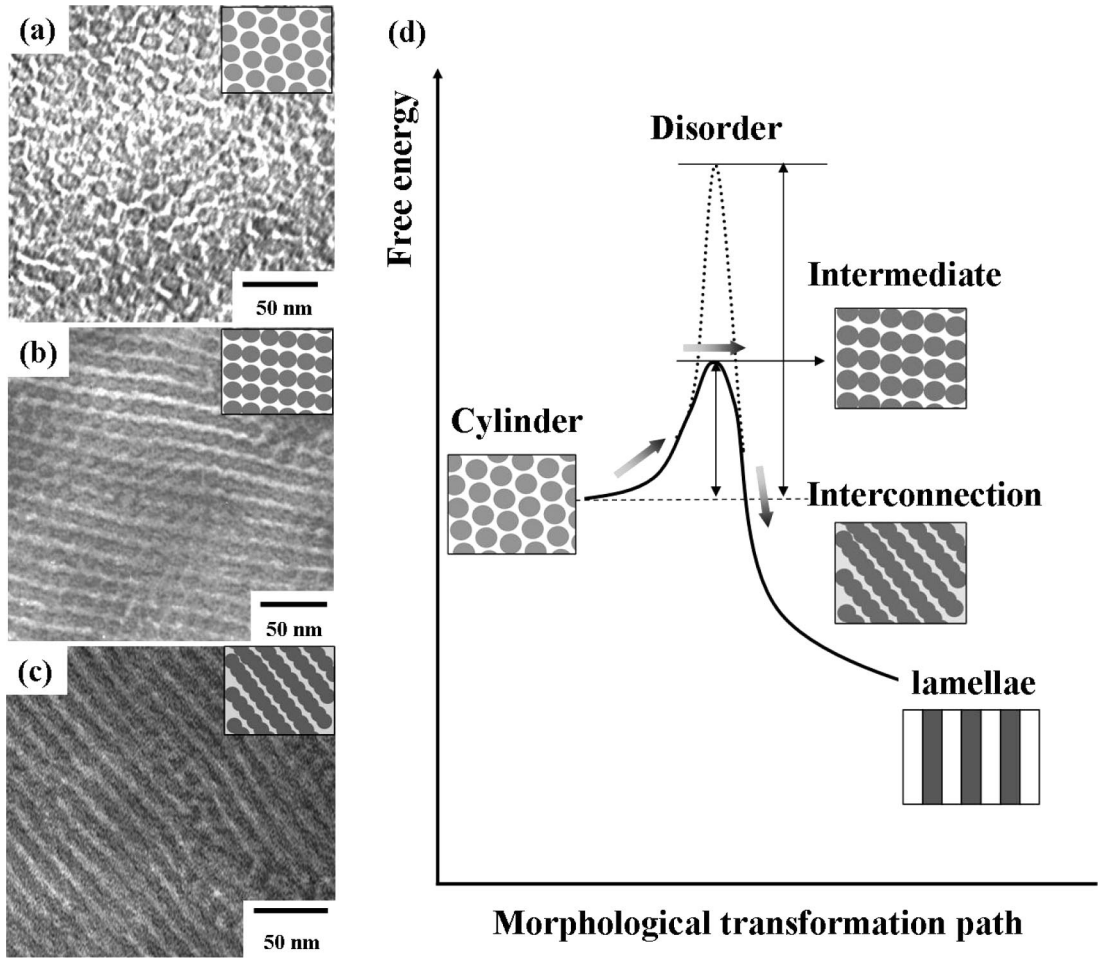

Figure 6. TEM micrographs of gold precursors/V2C7 (Au/N 1/30): (a) top view of the cylinder phase of pristine V2C7 ($f_{P4VP}{}^{\nu} = 0.24$), (b) observation of the interconnection between neighboring cylinders caused by the loading of gold precursors, and (c) observation of the interconnection-induced phase transformation from cylinder to lamellae. (d) Schematic representation of the change in the free energy with morphological transformation.

chains in the V2C7 ($f_{P4VP}{}^{\nu} = 0.24$) tend to stretch effectively so as to lead the phase transformation, as illustrated in Figure 7b1. Also, because of the significant stretching (i.e., a stiff initial slope in the plot of Figure 7a), the solubility limit can be easily reached in the V2C7 ($f_{P4VP}{}^{\nu} = 0.24$) hybrids. As observed, large amounts of the gold precursors might be excluded to the center of P4VP microdomains (as illustrated in Figure 7b2) to release the entropic penalty from the P4VP stretching further through particle−particle interaction. As a result, a decrease in the long period from 22.9 to 21.6 nm with the invariable PCL domain spacing can be observed in the V2C7 ($f_{P4VP}{}^{\nu} = 0.24$) hybrid with Au/N 1/3. In contrast, shorter intercylinder distance (7.4 nm) in the V4C7 ($f_{P4VP}{}^{\nu} = 0.38$) may release the entropic penalty through the interconnection of intercylinders. As a result, the large amounts of gold precursors could be significantly stabilized by P4VP stretching, in which the domain spacing of P4VP is gradually increased from 20.8 (Figure 7b3) to 22.4 nm (Figure 7b4). The variation in the domain spacings of the V4C7 ($f_{P4VP}{}^{\nu} = 0.38$) hybrids indicates that the swelling of the long period continues by the introduction of gold precursors and there is no occurrence of a solubility limit so as to lead the increase in the domain spacing of PCL (Figure 7b4). To examine the PCL blocking effect further, we used the V3C7 ($f_{P4VP}{}^{\nu} = 0.30$) with an intermediate intercylinder distance of 8.2 nm (Figure 7b5). Consistently, the stretching of P4VP chains, namely, the increase in effective excluded volume, is dependent on the intercylinder distance at which the initial slope in the plot of Figure 7a varies with the intercylinder distance (V2C7 > V3C7 > V4C7). The experimental results are consistent with the simulated phase diagram proposed by Lodge and coworkers.[20] Also, according to the simulation, the morphological stability of selective solvent/BCP mixtures can be improved by increasing the chain length of the prewetting block.

For the P4VP-rich P4VP-PCL hybrids, we speculate that the bridging for hybridized P4VP chains can be effectively achieved because of the low energy barriers for the interconnection of hybridized P4VP microdomains (i.e., short PCL chain for blocking). As schematically illustrated in Figure 8, we may start with the formation of dispersive, hybridized P4VP microdomains because of the selection of a neutral solvent for the PCL and the P4VP blocks but a nonsolvent for the gold precursors. In the PCL-rich P4VP-PCL hybrids, the rich PCL coverage of dispersive microdomains serves as the driving force for consolidating the microphase separation from the interruption of enormous bridging (Figure 8a). Consequently, the phase transformation can be induced through the bridging mechanism (this behavior has been discussed in Figure 6) in which the ordered nanostructures from microphase separation can be preserved by strong PCL blocking. In contrast, in the P4VP-rich P4VP-PCL hybrids, the driving force for bridging resulting from the strong association of the gold precursors and the P4VP block overwhelmingly prevailed against the driving force for the formation of ordered nanostructures (Figure 8b). Note that the binding energy of metal−ligand is several times larger than the van der Waals energy. Consequently, the coverage of short PCL brushes on the hybridized P4VP microdomains is insufficient against the strong interconnection of neighboring hybridized P4VP microdomains through bridging so as to result in disordered

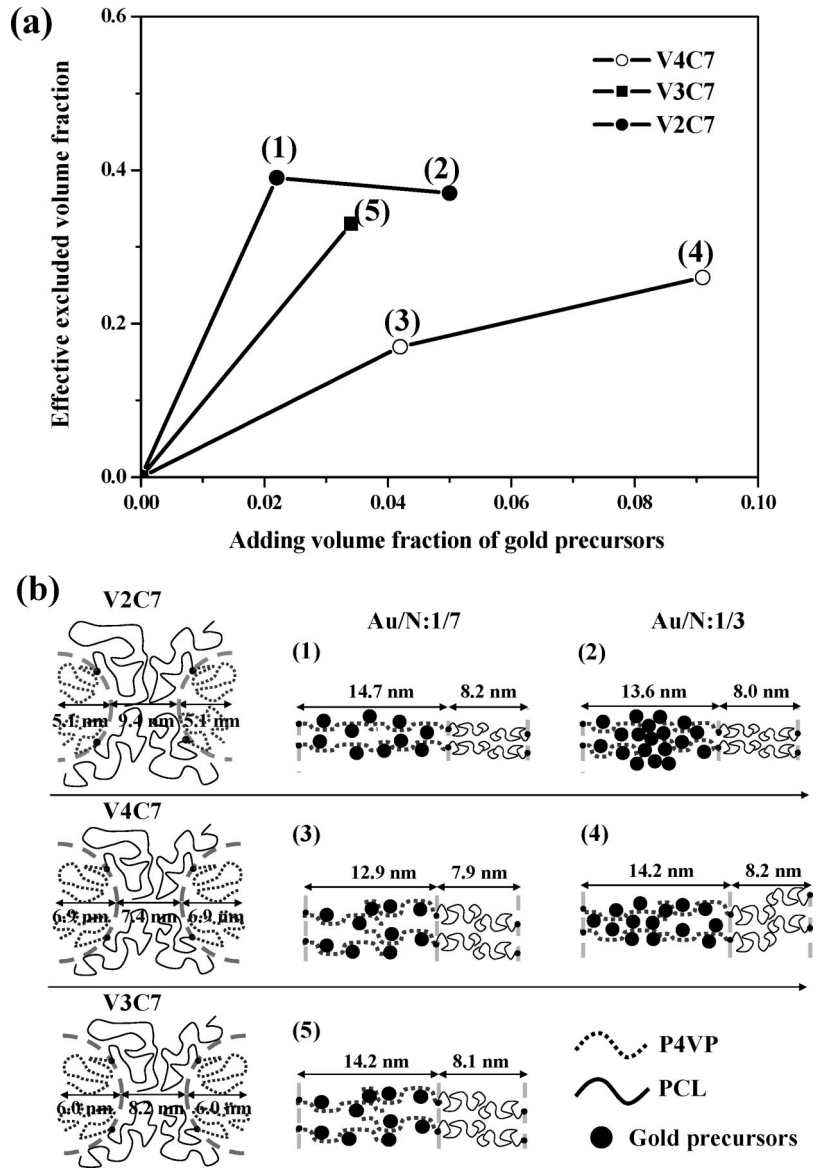

Figure 7. (a) The relation between the effective excluded volume of hybridized P4VP and the volume fraction of gold precursors in different hybrids. (b) Schematic representation of calculated results for PCL and P4VP domain spacings. In the V2C7 ($f_{P4VP}{}^{\nu} = 0.24$) hybrids, the long period of lamellar phase decreases from 22.9 nm (1) to 21.6 nm (2) with increasing the loading of gold precursors from Au/N 1/7 to 1/3. In the V4C7 ($f_{P4VP}{}^{\nu} = 0.38$) hybrids, the long period of lamellar phase increases from 20.8 (3) to 22.4 nm (4) with increasing the loading of gold precursors from Au/N 1/7 to 1/3. In the V3C7 ($f_{P4VP}{}^{\nu} = 0.3$) hybrid, the long spacing is ~22.3 nm (5).

texture. To examine the mutual interaction between the bridging and the PCL blocking effect further, a P4VP-PCL sample with symmetric constituent composition (i.e., V5C5 ($f_{P4VP}{}^{\nu} = 0.50$), that is, a lamellar phase) was synthesized for hybridization (Figure 9a). Similar results can be found in which significant distortion in the microphase-separated morphology occurs even with a very small amount of gold precursors introduced (Figure 9b), and no phase transformation could be identified. Consequently, in contrast with the occurrence of phase transformation for the PCL-rich P4VP-PCL hybrids, the introduction of the gold precursors gives rise to the formation of disordered morphology through the direct association of hybridized P4VP chains resulting from bridging against the formation of ordered nanostructure from microphase separation.

In summary, the phase behavior of the P4VP-PCL can be smoothly modified by the addition of inorganic precursors in the composition region with significant PCL blocking (that is, PCL-rich composition). The evolution of phase transformation in the P4VP-PCL hybrids agrees with the predicted phase behavior of inorganic nanoparticle/BCP hybrids[16] and homopolymer/BCP blends[19] as well as the selective solvent/BCP mixtures[20] while assuming that the chemical affinity of the additional species is equal to that of the of constituent block. However, the hybridized results in the P4VP-PCL hybrids indicate that the tendency for phase transformation is much more remarkable than that in the above systems because of the significant increase in the effective excluded volume. The dramatic change in the excluded volume by the introduction of the inorganic precursors is allegedly attributed to the multiattached sites for the strong association between the gold precursors and the P4VP block. In contrast to the phase transformation in the hybrids with PCL-rich P4VP-PCL fractions, disordered morphology can be found in the hybrids with P4VP-rich P4VP-PCL fractions. Because of the weak PCL blocking effect, the bridging mechanism for hybridization can be freely achieved through the strong association of hybridized P4VP chains. Consequently, the driving force for the formation of ordered nanostructures from microphase separation in the P4VP-rich P4VP-PCL fractions is effectively disrupted by hybridization, even with a small amount of introduced gold

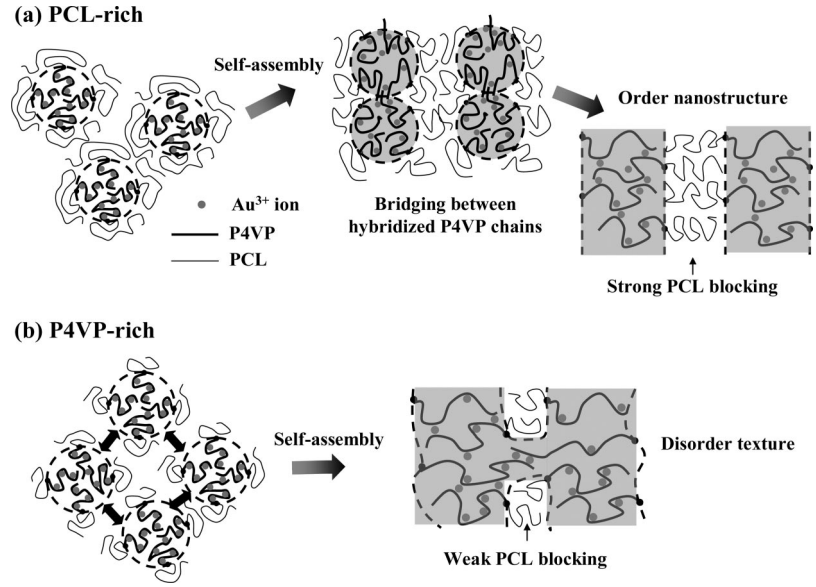

Figure 8. Schematic illustration of the bridging for hybridized P4VP chains and the PCL blocking effect in: (a) PCL-rich P4VP-PCL hybrids. The phase transformation can be induced by interconnection of hybridized P4VP microdomains through the bridging of hybridized P4VP chains in which the ordered nanostructures from microphase separation can be consolidated because of long PCL brushes, namely, strong PCL blocking. (b) P4VP-rich P4VP-PCL hybrids. The coverage of short PCL brushes on the hybridized P4VP microdomains is insufficient against the strong interconnection of neighboring hybridized P4VP microdomains through the bridging of hybridized P4VP chains (it is referred to as the weak PCL blocking) so as to result in disordered texture.

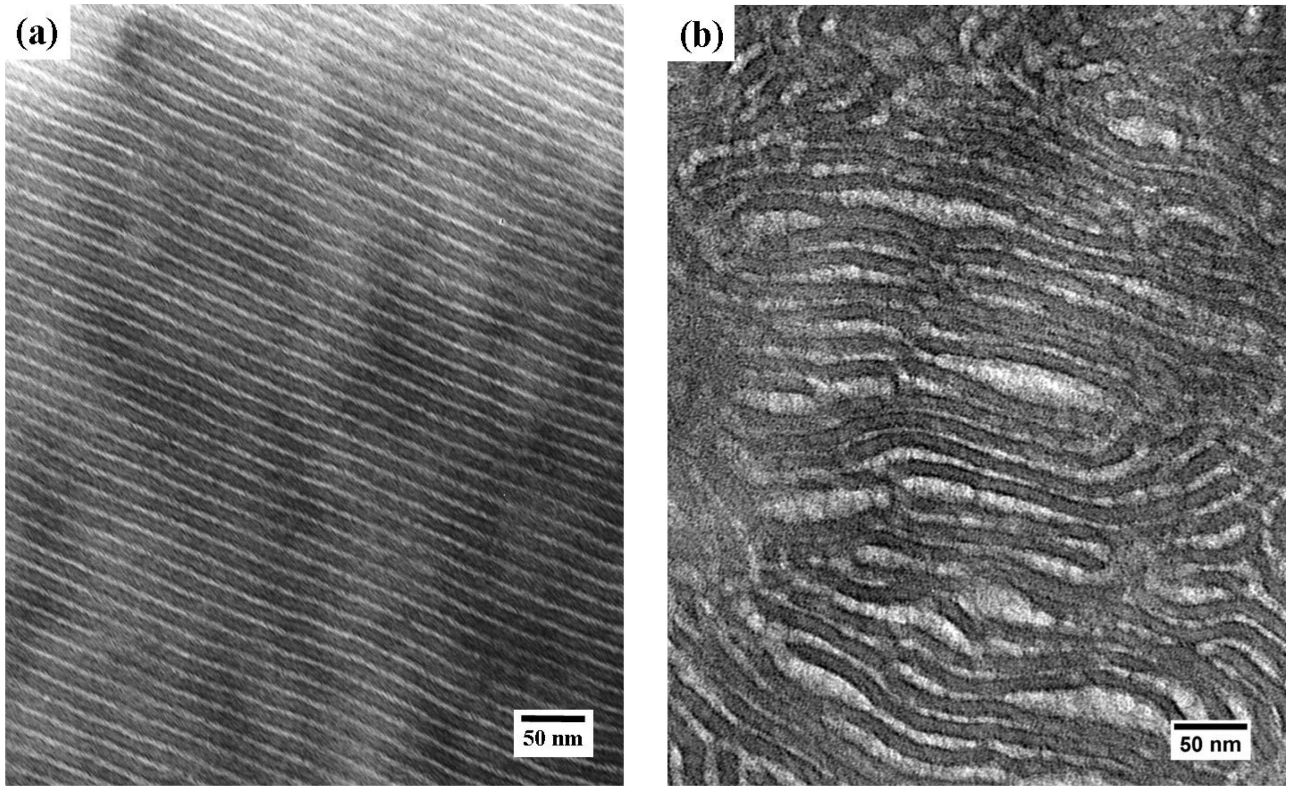

Figure 9. TEM micrographs of (a) V5C5 ($f_{P4VP}{}' = 0.5$) and (b) gold precursors/V5C5 (Au/N 1/14) with RuO_4 staining.

precursors. Interestingly, the phase behavior in the composition region with weak PCL blocking (that is, P4VP-rich composition) shows that the strong bridging tends to dominate the overall phase behavior of the hybrids. Obviously, the strong association between inorganic precursors and polymeric functional groups significantly varies the conformation of polymer chains in which this association likely overwhelms the repulsive force between constituent blocks for the formation of ordered nanostructures from microphase separation so as to result in the discrepancies with the predicted phase behavior of inorganic nanoparticle/BCP hybrids and homopolymer/BCP blends as well as the selective solvent/BCP mixtures.

Conclusions

The phase behavior of gold precursors/P4VP-PCL hybrids can be classified into two cases: (1) Phase transformation can be induced by the association between the gold precursors and

the P4VP block in the hybrids with the PCL-rich P4VP-PCL fractions. The introduction of the inorganic precursors to the BCPs gives rise to the change in the hybridized morphology from the cylinder phase to the lamellar phase with distorted textures. Moreover, the tendency for the phase transformation induced by the gold precursor seems to be more effective than that in the cases of the homopolymer/BCP blends and the selective solvent/BCP mixtures, as evidenced by the 1D SAXS correlation analysis, suggesting that the effective excluded volume of hybridized microdomains can be dramatically enhanced by the association between gold precursors and the P4VP block. For this unusual swelling behavior, we speculate that the dramatic change in the excluded volume is caused by the multiattached sites for the strong association between the gold precursors and the P4VP block. (2) Instead of phase transformation in the hybrids with PCL-rich P4VP-PCL fractions, disordered nanostructures were found in the hybrids with P4VP-rich P4VP-PCL fractions, suggesting that the strong association tends to dominate the overall phase behavior of the hybrids against the formation of ordered phase from microphase separation once the P4VP blocks appear to be the major content in P4VP-PCL samples.

Acknowledgment. This research was supported by the National Science Council (NSC) of Taiwan (NSC95-2221-E007-131-MY2) and the Electronics Research & Service Organization, Industrial Technology Research Institute (ITRI) of Taiwan. We thank Dr. B. S. Hsiao of the Chemistry Department, State University of New York at Stony Brook and Drs. U. S. Jeng and Y. S. Sun of the National Synchrotron Radiation Research Center (NSRRC) for their help in Synchrotron SAXS experiments.

Supporting Information Available: TEM images and corresponding SAXS profiles of all P4VP-PCL samples used in this study. This material is available free of charge via the Internet at http://pubs.acs.org.

References and Notes

(1) Spatz, J. P.; Roescher, A.; Moller, M. *Adv. Mater.* **1996**, *8*, 337.
(2) Forster, S.; Antonietti, M. *Adv. Mater.* **1998**, *10*, 195.
(3) Thurn-Albrecht, T.; Schotter, J.; Kastle, G. A.; Emley, N.; Shibauchi, T.; Krusin-Elbaum, L.; Guarini, K.; Black, C. T.; Tuominen, M. T.; Russell, T. P. *Science* **2000**, *290*, 2126.
(4) Lopes, W. A.; Jaeger, M. *Nature* **2001**, *414*, 735.
(5) Bockstaller, M. R.; Kolb, R.; Thomas, E. L. *Adv. Mater.* **2001**, *13*, 1783.
(6) Ribbe, A. E.; Okumura, A.; Matsushige, K.; Hashimoto, T. *Macromolecules* **2001**, *34*, 8239.
(7) Sohn, B. H.; Seo, B. H. *Chem. Mater.* **2001**, *13*, 1752.
(8) Boontongkong, Y.; Cohen, R. E. *Macromolecules* **2002**, *35*, 3647.
(9) Abes, J. I.; Cohen, R. E.; Ross, C. A. *Chem. Mater.* **2003**, *15*, 1125.
(10) Yeh, S. W.; Wei, K. H.; Sun, Y. S.; Jeng, U. S.; Liang, K. S. *Macromolecules* **2005**, *38*, 6559.
(11) Bockstaller, M. R.; Thomas, E. L. *Phys. Rev. Lett.* **2004**, *93*, 166106.
(12) Li, H.; Eddaoudi, M.; O'Keeffe, M.; Yaghi, O. M. *Nature* **1999**, *402*, 276.
(13) He, Y.; Lodge, T. P. *Macromolecules* **2008**, *41*, 167.
(14) Cho, J. H.; Lee, J.; He, Y.; Kim, B.; Lodge, T. P.; Frisbie, C. *Adv. Mater.* **2008**, *20*, 686.
(15) Yaghi, O. M.; Li, G.; Li, H. *Nature* **1995**, *378*, 703.
(16) Huh, J.; Ginzburg, V. V.; Balazs, A. C. *Macromolecules* **2000**, *33*, 8085.
(17) Thompson, R. B.; Ginzburg, V. V.; Matsen, M. W.; Balazs, A. C. *Science* **2001**, *292*, 2469.
(18) Matsen, M. W.; Thompson, R. B. *Macromolecules* **2008**, *41*, 1853.
(19) Hashimoto, T.; Tanaka, H.; Hasegawa, H. *Macromolecules* **1990**, *23*, 4378.
(20) Lodge, T. P.; Pudil, B.; Hanley, K. J. *Macromolecules* **2002**, *35*, 4707.
(21) Bockstaller, M. R.; Lapetnikov, Y.; Margel, S.; Thomas, E. L. *J. Am. Chem. Soc.* **2003**, *125*, 5276.
(22) Kim, B. J.; Chiu, J. J.; Yi, G.; Pine, D. J.; Kramer, E. J. *Adv. Mater.* **2005**, *17*, 2618.
(23) Huang, C. M.; Wei, K. H.; Jeng, U. S.; Liang, K. S. *Macromolecules* **2007**, *40*, 5067.
(24) Lo, C. T.; Lee, B.; Pol, V. G.; Rago, N. L. D.; Seifert, S.; Winans, R. E.; Thiyagarajan, P. *Macromolecules* **2007**, *40*, 8302.
(25) Adachi, M.; Okumura, A.; Sivaniah, E.; Hashimoto, T. *Macromolecules* **2006**, *39*, 7352.
(26) Ho, R. M.; Lin, T.; Jhong, M. R.; Chung, T. M.; Ko, B. T.; Chen, Y. C. *Macromolecules* **2005**, *38*, 8607.
(27) Lee, D. H.; Kim, H. Y.; Kim, J. K.; Huh, J.; Ryu, D. Y. *Macromolecules* **2006**, *39*, 2027.
(28) He, Y.; Li, Z.; Simore, P.; Lodge, T. P. *J. Am. Chem. Soc.* **2006**, *128*, 2745.
(29) Simore, P.; Lodge, T. P. *Macromolecules* **2008**, *41*, 1753.
(30) Lodge, T. P. *Science* **2008**, *4*, 50.
(31) Wang, J. P.; Chen, W.; Roy, C.; Sievert, J. D.; Russell, T. P. *Macromolecules* **2008**, *41*, 963.
(32) Wang, J. P.; Chen, W.; Russell, T. P. *Macromolecules* **2008**, *41*, 4904.
(33) Ko, B. T.; Lin, C. C. *Macromolecules* **1999**, *32*, 8296.
(34) Xia, J.; Zhang, X.; Matyjaszewski, K. *Macromolecules* **1999**, *32*, 3531.
(35) Sun, Y. S.; Chung, T. M.; Li, Y. J.; Ho, R. M.; Ko, B. T.; Jeng, U. S.; Lotz, B. *Macromolecules* **2006**, *39*, 5782. According to the method for determining χ by measuring the characteristic domain spacing (D_{lam}) from SAXS patterns for lamellar morphology, symmetric BCP P4VP-*b*-PCL (VP/CL 47/46, $f'_{PCL} = 0.5$) served to determine the temperature dependence of χ that is described by $\chi(T) = 103.48/T - 0.062$. The order−disorder-transition temperatures for P4VP-*b*-PCL samples tested here were determined from SAXS at various temperature ⩾120 °C to avoid nonequilibrium effects below the glass transition of P4VP. The synthesized BCP is not expected to disorder up to their decomposition point (>200 °C) on the basis of the block chain length and in situ SAXS evidence.
(36) Hunter, R. J. *Foundations of Colloid Science*; Oxford University Press: New York, 1987.
(37) Sakurai, S.; Momii, T.; Taie, K.; Shibayama, M.; Nomura, S.; Hashimoto, T. *Macromolecules* **1993**, *26*, 485.

MA8015618